Journal of Power Sources 195 (2010) 6524–6531

Contents lists available at ScienceDirect

Journal of Power Sources

journal homepage: www.elsevier.com/locate/jpowsour

Raney-platinum film electrodes for potentially implantable glucose fuel cells. Part 2: Glucose-tolerant oxygen reduction cathodes

S. Kerzenmacher[a,*], U. Kräling[a], M. Schroeder[b], R. Brämer[c], R. Zengerle[a,d], F. von Stetten[a]

[a] Laboratory for MEMS Applications, Department of Microsystems Engineering - IMTEK, University of Freiburg, Georges-Koehler-Allee 106, 79110 Freiburg, Germany
[b] Institut für Anorganische und Analytische Chemie, University of Freiburg, Albertstrasse 21, 79104 Freiburg, Germany
[c] Hochschule Offenburg - University of Applied Sciences, Badstrasse 24, 79652 Offenburg, Germany
[d] Centre for Biological Signalling Studies (bioss), Albert-Ludwigs-Universität Freiburg, Germany

ARTICLE INFO

Article history:
Received 22 January 2010
Received in revised form 9 April 2010
Accepted 13 April 2010
Available online 22 April 2010

Keywords:
Glucose fuel cell
Implantable
Raney
Platinum
Aluminum
Artificial tissue fluid

ABSTRACT

We report the fabrication and characterization of glucose-tolerant Raney-platinum cathodes for oxygen reduction in potentially implantable glucose fuel. Fabricated by extraction of aluminum from 1 μm thin platinum–aluminum bi-layers annealed at 300 °C, the novel cathodes show excellent resistance against hydrolytic and oxidative attack. This renders them superior over previous cathodes fabricated from hydrogel-bound catalyst particles. Annealing times of 60, 120, and 240 min result in approximately 400–550 nm thin porous films (roughness factors ∼100–150), which contain platinum and aluminum in a ratio of ∼9:1. Aluminum release during electrode operation can be expected to have no significant effect on physiological normal levels, which promises good biocompatibility. Annealing time has a distinct influence on the density of trenches formed in the cathode. Higher trench densities lead to lower electrode potentials in the presence of glucose. This suggests that glucose sensitivity is governed by mixed potential formation resulting from oxygen depletion within the trenches. During performance characterization the diffusion resistance to be expected from tissue capsule formation upon electrode implantation was taken into account by placing a membrane in front of the cathode. Despite the resulting limited oxygen supply, cathodes prepared by annealing for 60 min show more positive electrode potentials than previous cathodes fabricated from hydrogel-bound activated carbon. Compared to operation in phosphate buffered saline containing 3.0 mM glucose, a potential loss of approximately 120 mV occurs in artificial tissue fluid. This can be reduced to approximately 90 mV with a protective Nafion layer that is easily electro-coated onto the Raney-platinum film.

© 2010 Elsevier B.V. All rights reserved.

1. Introduction

Raney-platinum film electrodes posses a number of advantages over conventional hydrogel-bound particle electrodes commonly used in abiotically catalyzed implantable glucose fuel cells [1]. These comprise [2,3] high catalytic activity for anodic glucose oxidation, excellent resistance against oxidative and hydrolytic attack, and the amenability to versatile surface modification with protective polymer layers [2].

While platinum exhibits high catalytic activity also for oxygen reduction [4], corresponding Raney-type film cathodes have to date not been applied in implantable glucose fuel cells. This may be related to the simultaneous presence of glucose and oxygen in physiological environments. Under such conditions ∼10–100 μm thick porous platinum-based electrodes exhibit mixed potentials closer to the redox potential of glucose oxidation [5–7]. As illustrated schematically in Fig. 1, this can be explained by oxygen consumption on the catalytically active platinum surface in the outer region of the electrode [1], either by the direct chemical reaction of oxygen with glucose or the electro-reduction of oxygen to water in case the electrode is operated as fuel cell cathode. In the oxygen-depleted interior of the cathode the local potential is then dominated by the presence of glucose, which can drastically lower fuel cell voltage and thus power output.

Previous approaches to solve this problem employ for instance glucose insensitive oxygen reduction catalysts such as activated carbon [8,9] or silver [9,10]. Alternatively, hydrophobic membranes [6,11] have been placed in front of platinum cathodes to hinder glucose access. Both approaches come with several disadvantages [1]: while activated carbon and silver exhibit lower catalytic activity for oxygen reduction than platinum, the concept with hydrophobic membranes mandates reactant access to the fuel cell from two sides. This renders mounting of the fuel cell directly on the casing of a medical implant difficult.

We suggest to circumvent the interference of glucose oxidation with cathodic oxygen reduction by the construction of sufficiently

* Corresponding author. Tel.: +49 761 203 7328; fax: +49 761 203 7322.
E-mail address: kerzenma@imtek.de (S. Kerzenmacher).

0378-7753/$ – see front matter © 2010 Elsevier B.V. All rights reserved.
doi:10.1016/j.jpowsour.2010.04.049

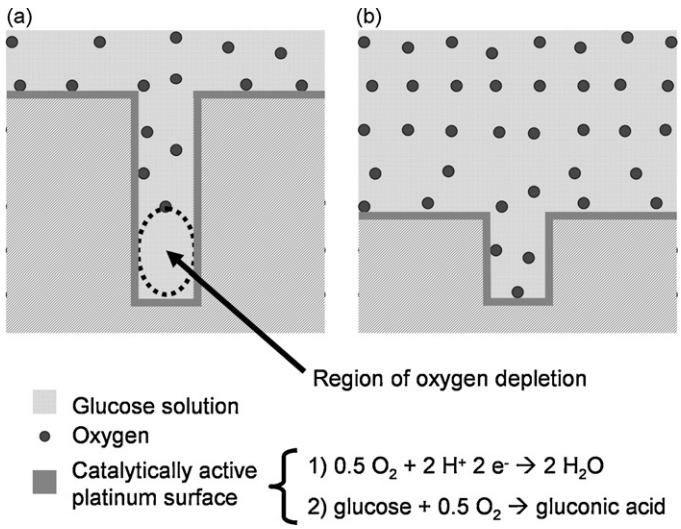

Fig. 1. Schematic illustration of oxygen availability in porous platinum cathodes of different thicknesses. (a) Thick layer: oxygen is fully consumed in the outer region of the pore (either by (1) electro-reduction to water or by (2) direct chemical reaction with glucose). In the oxygen-depleted interior of the electrode the local potential is dominated by the redox potential of glucose oxidation. (b) Thin layer: sufficient oxygen to prevent the formation of anoxic regions can diffuse into the pore.

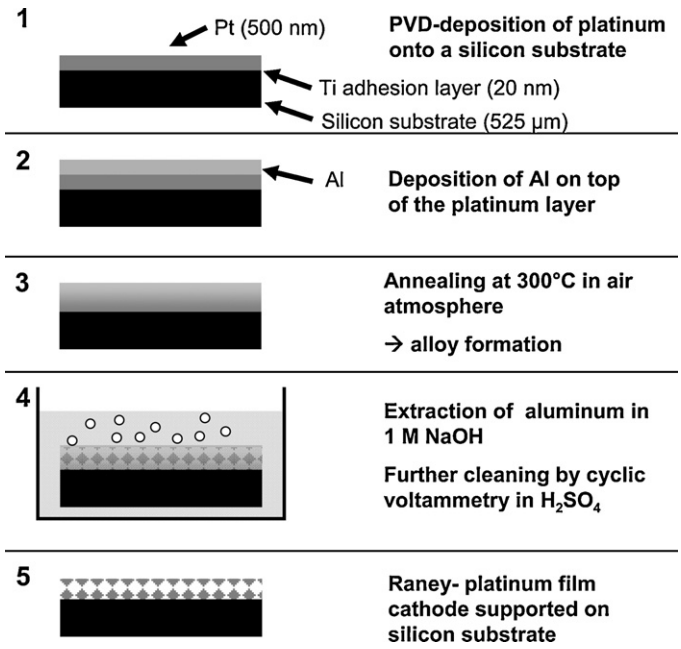

Fig. 2. Schematic of the cathode fabrication processes. See text for explanations.

thin, porous platinum electrodes. As illustrated in Fig. 1, a sufficiently thin enough electrode would prevent the formation of oxygen-depleted regions within the cathode and thus decrease the extent of mixed potential formation. According to this concept we here investigate the fabrication and applicability of Raney-platinum electrodes as chemically resistant and glucose-tolerant oxygen reduction cathodes for implantable glucose fuel cells. An attractive possibility to fabricate sub-micrometer thin Raney-type platinum electrodes is the annealing of PVD-deposited bi-layers of platinum and an extractable metal [12–14]. As extractable metal forming alloys with platinum we chose aluminum [15], due to its established use and thus ready availability as sputtering target for the PVD (physical vapor deposition) process. The electrode materials formed upon different annealing times are characterized by means of X-ray diffraction (XRD), X-ray photoelectron spectroscopy (XPS), and energy-dispersive X-ray spectroscopy (EDX). Their oxygen reduction performance under physiological concentrations of glucose and oxygen is characterized by recording current density–potential curves in both, phosphate buffered saline and artificial tissue fluid. To account for the limited oxygen supply to be expected from tissue encapsulation upon implantation an appropriate diffusion barrier is placed in front of the cathode. Included into the study is the analysis of aluminum leaching upon prolonged operation, and a first step towards improving cathode performance in terms of glucose sensitivity and tolerance towards artificial tissue fluid by application of a protective Nafion coating [16–18].

2. Experimental

2.1. Fabrication of Raney-platinum cathodes

The individual fabrication steps are schematically illustrated in Fig. 2, and described in the following. As substrate for metal deposition 525 μm thick silicon wafers (native oxide removed in 1% HF, orientation ⟨1 0 0⟩ , n+ doped with phosphorus, 100 mm diameter, Siltronix, Archamps, France) were used.

Electrodes were prepared by firstly evaporating a 20 nm thin titanium adhesion layer on the silicon substrate, followed by 500 nm platinum and a final 500 nm aluminum layer. During subsequent dicing of the wafer into 17 mm × 17 mm chips the thin metal surface was protected with approximately 2 μm photoresist that was afterwards removed. Following this, the chips were annealed at 300 °C in air atmosphere for 60, 120, or 240 min. In accordance with annealing time these samples are designated as $Pt–Al_{60}$, $Pt–Al_{120}$, and $Pt–Al_{240}$, respectively. Subsequently the samples were immersed in 1 M NaOH (Merck KGaA, Darmstadt, Germany) for approximately 15 min to extract aluminum from the alloy. Further cleaning was achieved by 20 cyclic voltammetry sweeps in de-aerated 0.5 M H_2SO_4 (Merck KGaA, Darmstadt, Germany). The scan rate was 50 mV s^{-1} between 1.3 and −0.3 V vs. a saturated calomel reference electrode (SCE).

2.2. Nafion modification

$Pt–Al_{60}$ cathodes were modified by an approximately 300 nm thin electro-coated Nafion layer on top of the porosified platinum layer according to the procedure reported elsewhere [2]. In short, the sample was immersed in Nafion solution (5% Nafion 521, Quintech, Göppingen, Germany) and a potential of +1.5 V was applied between the cathode and a platinum wire counter electrode (Ø 1 mm, 40 mm long, Chempur, Karlsruhe, Germany). After 120 s the sample was pulled out of the solution at 40 mm min^{-1} while maintaining the potential at +1.5 V. Subsequently, the Nafion layer was cured at 70 °C for 30 min.

2.3. Microstructural evaluation

Roughness factors were estimated from the charge under the hydrogen desorption peaks in the cyclic voltammograms as described in Ref. [2]. Also the determination of platinum to aluminum ratios of the Raney-platinum electrodes (after operation) by means of energy-dispersive X-ray (EDX) analysis was performed as previously described [2]. The results are presented together with the sample standard variation, given in parentheses.

Cross-sections were prepared using an Ar-ion beam cross-section polisher (SM-09010, Jeol GmbH, Eching, Germany) and observed with a Zeiss Supra 60 VP scanning electron microscope operating at 5 kV.

The intermetallic phases present in the porosified platinum layers were identified by X-ray powder diffraction, using a PSD

(Position Sensitive Detector) transmission diffraction system (Stoe, Darmstadt, Germany) with Cu Kα radiation. Thereto samples have been prepared as described in Section 2.1, but on a 500 μm thick borosilicate glass wafer (V015.04-003, Planoptik AG, Elsoff, Germany) with similar thermal expansion coefficient as the silicon wafer used for electrode fabrication. From the glass wafer the thin porosified platinum films were easily transferable to a strip of adhesive tape that also served as sample support during analysis. Eight individual patterns in 2Θ range between 20° and 90° were recorded with an exposure time of 800 s, resulting in reflections with high intensity. To suppress artifacts, the eight individual patterns were added up to a single pattern.

X-ray photoelectron spectra (XPS) were recorded between 0 and 1200 eV, using Mg Kα radiation at 300 W (5600 ci, Physical Electronics Inc., Chanhassen, MN). Thereto the samples (plan view) were Ar-sputtered (PerkinElmer 11-065 ion gun operating at 3 kV) for 5 and 10 s to remove surface contaminants from preceding operation. The detected area was 800 μm in diameter; the detector angle was 45°.

Since the electrodes of implantable glucose fuel cells are in direct contact with body fluids, also their biocompatibility has to be considered. Electrolyte samples for the analysis of aluminum release from the $Pt–Al_{60}$ electrode upon operation were obtained in separate experiments, as previously described [2]. Thereto a cathode of 2.25 cm^2 in size was operated for 10 days at a constant current of 40 μA in 100 ml of aerated phosphate buffered saline (PBS tabs, Invitrogen, Karlsruhe, Germany) containing 3.0 mM glucose. The cathode has been operated before (during the screening of fabrication parameters), and was thus not further cleaned by treatment with an oxidative current. Subsequently the concentration of aluminum in the testing solution was analyzed by graphite-furnace atomic absorption spectroscopy (Model 1100B, PerkinElmer, Waltham, MA), using a single-element hollow cathode lamp. The analysis of the testing solution was repeated eight times, the result is given as (mean value ± sample standard deviation). In this experiment, the volume of 100 ml is approximately only 7% of the tissue fluid volume that would be required to sustain the fuel cell's oxygen consumption over 10-day operation period. This procedure leads to an approximately 15-fold aluminum concentration in the testing solution as compared to actual operation of the fuel cell in a physiological environment. This was taken into consideration when evaluating the significance of aluminum leaching from the electrode by comparison to physiological normal concentrations in serum.

2.4. Electrode assembly with diffusion barrier

Since our earlier studies [8] indicate that in the physiological range oxygen mass transfer to the cathode becomes performance limiting, it is necessary to consider the additional diffusion resistance expected from tissue capsule formation around implanted foreign bodies. Based on the work of Sharkawy et al. [19] the diffusion resistance of fluorescein through a tissue capsule can be estimated to be in the range between 2.5×10^4 s cm^{-1} (tissue thickness d = 250 μm, $D^{\text{eff}}_{\text{Fluorescein}} = 1 \times 10^{-6}$ cm^2 s^{-1}) and 5×10^3 s cm^{-1} (tissue thickness d = 100 μm, $D^{\text{eff}}_{\text{Fluorescein}} = 2 \times 10^{-6}$ cm^2 s^{-1}).

To account for this additional diffusion resistance, a 136 μm thick porous membrane (Supor-450, Pall Life Sciences, East Hills, NY) was placed in front of the electrodes during performance characterization. This membrane's effective diffusion coefficient for glucose at 37 °C (after autoclaving at 121 °C for 15 min) has been determined in a classical two-chamber diffusion experiment [20] under continuous stirring. Thereto the porous filter membrane was clamped between a chamber filled with 25 ml PBS and a second chamber filled with 25 ml PBS containing 5.0 mM glucose. Over a period of 6 h the concentration change in both chambers was followed by regularly taking three samples of 25 μl from each chamber, and analyzing their glucose concentration using a colorimetric [21] glucose assay (QuantiChrom, BioAssay Systems, Hayward, CA). The effective diffusion coefficient $D^{\text{eff}}_{\text{Glucose}}$ was then calculated according to

$$D^{\text{eff}}_{\text{Glucose}} = \frac{1}{t} \cdot \frac{d}{A} \cdot \frac{V_{\text{Chamber}}}{2} \cdot \ln\left(\frac{c^0_{\text{lower}} - c^0_{\text{upper}}}{c_{\text{lower}} - c_{\text{upper}}}\right)$$

wherein A is the membrane's area, d is its thickness, and V_{Chamber} is the volume of one chamber (25 ml). Furthermore, c^0_{upper} and c^0_{lower} are the initial concentrations in the chamber with and without glucose, respectively, whereas c_{upper} and c_{lower} are the corresponding glucose concentrations measured at time t. From three independent experiments an effective diffusion coefficient $D^{\text{eff}}_{\text{Glucose}} = (2.8 \pm 0.2) \times 10^{-6}$ cm^2 s^{-1} was determined, corresponding to a diffusion resistance of $(4.8 \pm 0.3) \times 10^3$ s cm^{-1}. This value is in the range of the above calculated diffusion resistance range for a typical tissue capsule, in particular when considering the larger molecular weight of fluorescein (Mw = 376 g mol^{-1}) as compared to glucose (Mw = 198 g mol^{-1}), To mount the electrodes together with the diffusion barrier previously reported [22] electrode fixtures were used, exposing a 2.25 cm^2 section of the electrode. The influence of contact resistance was eliminated by using separate platinum wires for electrode current and voltage.

Assembly and autoclavation of the electrodes in an aseptic electrochemical reactor [22] followed the procedure already described in Ref. [2]. Possible deposits formed during autoclavation were removed by operation the cathodes for 1 h in phosphate buffered saline (7.0% oxygen saturation) at an *oxidative* current density of 44 μA cm^{-2}. After this procedure, the testing solution was replaced with freshly prepared PBS. The complete setup was installed in an incubator to maintain the testing solution at a constant temperature of (37 ± 1) °C.

2.5. Performance characterization

For performance characterization the testing environment described elsewhere [22] was employed. In short, the electrodes were connected to the individual channels of a computer controlled current sink (STG 2008, Multichannel Systems, Reutlingen, Germany) operating in galvanostatic mode. The electrode potentials were recorded in 5-min intervals against a saturated calomel reference electrode (KE11, Sensortechnik, Meinsberg, Germany). The oxygen concentration in the aseptic electrochemical reactor was adjusted to either 3.5% or 7.0% oxygen saturation by mixing corresponding amounts of air and nitrogen with variable area flowmeters (Model 112-02TA, Analyt-MTC, Müllheim, Germany; estimated accuracy: ±0.2 percentage points in terms of oxygen saturation; total flow: 2 L min^{-1}).

For the analysis of different cathode fabrication parameters rapid multi-step chronopotentiometry experiments were performed. Starting from 0.0 μA cm^{-2} (open circuit) to a maximum value of 24.2 μA cm^{-2}, the current density was increased in steps of 8.8 μA cm^{-2} every hour. These experiments were performed first in phosphate buffered saline without glucose at 7.0% (data not shown) and 3.5% oxygen saturation, and then repeated at 3.5% oxygen saturation with additionally 3.0 mM glucose in the testing solution. To exclude the influence of electrode history all samples underwent the same experimental sequence. For clarity only the cathode potentials at open circuit and area specific resistances are reported instead of the complete current density–potential plots. The area specific resistances were calculated from the linear slope of the current density–potential curve between 0.0 μA cm^{-2} (open circuit) and 8.8 μA cm^{-2}.

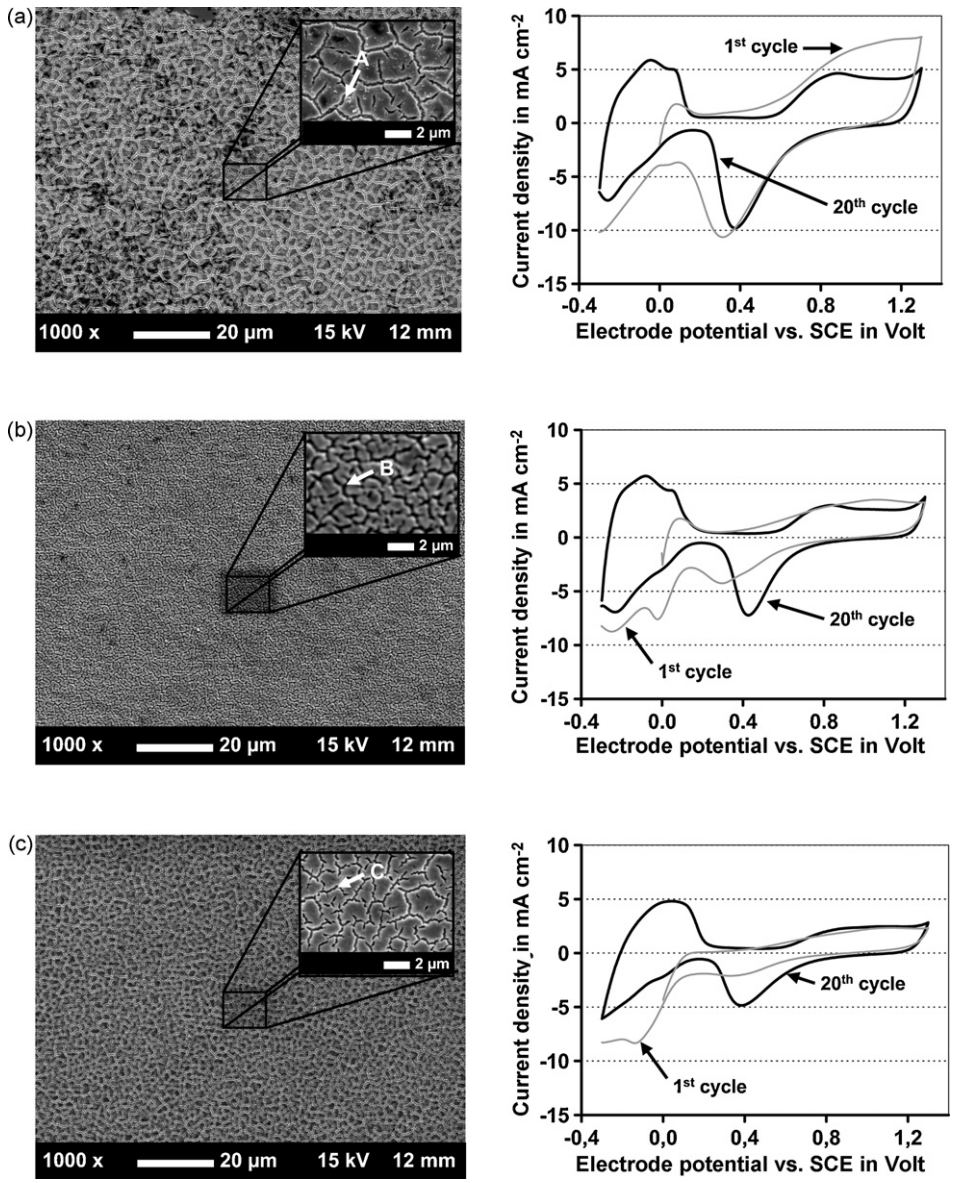

Fig. 3. Plan view micrographs (left) and corresponding cyclic voltammograms (right) in de-aerated H_2SO_4, shown for (a) *Pt–Al*$_{60}$, (b) *Pt–Al*$_{120}$ and (c) *Pt–Al*$_{240}$.

In addition, *Pt–Al*$_{60}$ samples with and without protective Nafion coating underwent a multi-step chronopotentiometry experiments with smaller load steps. Thereto current density was increased from 0.0 $\mu A\,cm^{-2}$ (open circuit) to a maximum value of 17.6 $\mu A\,cm^{-2}$ in steps of 2.2 $\mu A\,cm^{-2}$. Current density–potential plots were then constructed from the cathode potentials recorded after 12 h of operation at a given load current. The testing medium throughout these experiments was PBS containing 3.0 mM glucose, at oxygen saturations of 3.5% and 7.0%. Furthermore, these electrodes underwent a subsequent chronopotentiometry experiment where the current density was kept constant at 4.4 $\mu A\,cm^{-2}$ for approximately 26 h. The testing solution in this experiment was firstly PBS containing 3.0 mM glucose at 7.0% oxygen saturation. Subsequently the experiment was repeated in artificial tissue fluid (made from PBS with 3.0 mM glucose and amino acids as well as taurine at physiological concentration), as described in Ref. [2].

Throughout the paper roughness factors and potentials are reported as (mean value ± sample standard deviation), whereas bars in graphs represent the minimum and maximum value from triplicate experiments.

3. Results and discussion

3.1. Microstructural evaluation

In Fig. 3 plan view surface micrographs of the samples after alloy extraction and operation in PBS containing 3.0 mM glucose are shown, together with a representative cyclic voltammogram of the respective sample (1st and 20th cycle) recorded in de-aerated 0.5 M H_2SO_4.

The surface of all investigated samples shows a “mud-crack”-type pattern with distinctive trenches. Its microstructure is significantly affected by annealing time. In the case of *Pt–Al*$_{60}$ and *Pt–Al*$_{120}$ the trenches are typically between 200 and 400 nm wide (arrows A and B in Fig. 4), respectively. The longer annealing time of *Pt–Al*$_{240}$ results in smaller trenches of typically 100 nm width (arrow C in Fig. 4). From the digital electron micrographs (small

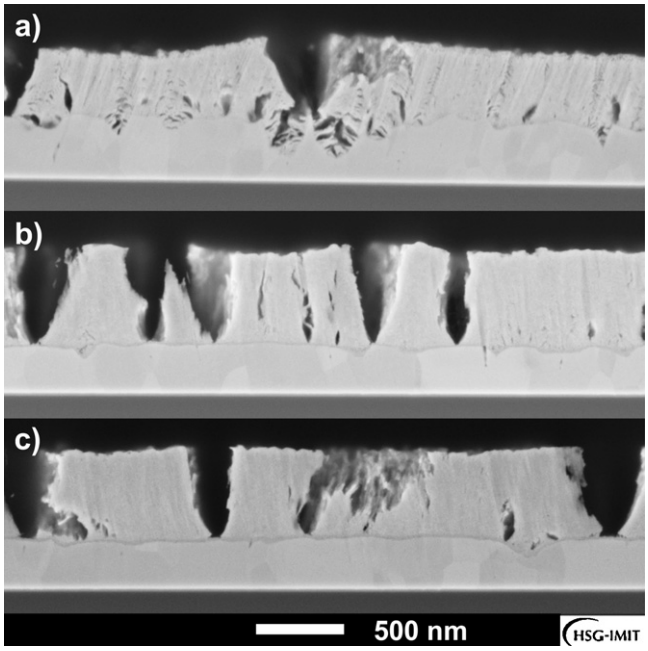

Fig. 4. Cross-sectional views of (a) *Pt–Al*$_{60}$, (b) *Pt–Al*$_{120}$ and (c) *Pt–Al*$_{240}$.

insets in Fig. 4) the mean trench densities were estimated by manually coloring the trenches and transforming the image into a two-tone image (performed with Photoshop 7.0.1, Adobe Systems Inc., San Jose, CA). Using the software's histogram function the share of the projected trench area on the total sample area was quantified. The lowest trench density of approximately 10% is observed for *Pt–Al*$_{60}$, whereas with *Pt–Al*$_{120}$ and *Pt–Al*$_{240}$ approximately 30% and 20% of the projected electrode area is occupied with trenches, respectively.

Regarding the cyclic voltammograms (Fig. 3), all samples show in principle the electrochemical behavior of platinum, with hydrogen peaks below a potential of 0.2 V vs. SCE as well as the peaks for platinum oxidation and reduction. The relatively broad peaks and their poor separation in the hydrogen area are attributed to the porous nature of the material. Stabilization of the cyclic voltammograms over the course of 20 cycles indicates the formation of chemically stable alloys.

Compared to un-annealed samples with a roughness factor of (13 ± 1), alloy formation and subsequent extraction of the non-noble component results in an approximately 10-fold increase in surface roughness. The roughness factors of *Pt–Al*$_{60}$ and *Pt–Al*$_{120}$ do not differ significantly, amounting to (135 ± 13) and (149 ± 3), respectively. *Pt–Al*$_{240}$ exhibits an only slightly lower roughness factor of (109 ± 14). These values are about twice the roughness factor reported by van der Wal et al. (~60 for annealing times of 60 and 120 min at 300 °C [14]), and can be explained by the thicker layers of platinum (750 nm) and aluminum (1.3 μm) as well as a different etchant to remove aluminum used in their work.

Fig. 4 shows the polished cross-sections of the porosified layers. The thickness of the porous layer and the trench depth depend only slightly on annealing time, increasing from approximately 400 nm for *Pt–Al*$_{60}$, to 550 and 500 nm for *Pt–Al*$_{120}$ and *Pt–Al*$_{240}$, respectively. With all samples a polycrystalline bulk platinum layer remains underneath the porosified structure. Its approximate thickness amounts to 350 nm for *Pt–Al*$_{60}$ and 300 nm for both, *Pt–Al*$_{120}$ and *Pt–Al*$_{240}$.

The remaining aluminum share in the micro-porous platinum films (obtained from EDX analysis after operation as cathode in PBS with 3.0 mM glucose) differs only marginally, amounting to platinum to aluminum ratios of 10.0:1.0 (±0.5) for *Pt–Al*$_{60}$, 8.0:1.0 (±0.5) for *Pt–Al*$_{120}$, and 8.1:1.0 (±0.4) for *Pt–Al*$_{240}$. Throughout the analysis no significant traces of silicon and titanium were detected, indicating that the active electrode layer solely consists of platinum and aluminum.

In Fig. 5 the XRD patterns of *Pt–Al*$_{60}$, *Pt–Al*$_{120}$, and *Pt–Al*$_{240}$ are compared, together with the theoretical pattern of crystalline Pt [23] (data taken from the ICSD – Inorganic Crystal Structure Database [24], FIZ, Karlsruhe, Germany). As with the Pt–Zn anodes investigated in the first part of this paper series [2], the diffraction patterns do not differ significantly between the investigated annealing times. Similarly, the XPS spectra of the different samples shown in Fig. 5b are in good agreement. This corresponds to the EDX results and indicates similar compositions of the porosified layer for all investigated samples.

Since EDX analysis points towards platinum to aluminum ratios in the range of 9:1, also the intermetallic compound $Pt_{0.9}Al_{0.1}$ was taken into consideration. However, due to the closely related crystal structures of Pt (Cu-type, $Fm\bar{3}m$, $a = 3.924$ Å [23]) and $Pt_{0.9}Al_{0.1}$ (Cu-type, $Fm\bar{3}m$, $a = 3.906$ Å [23]) it is difficult to differentiate between their diffraction patterns in a graphical representation (Fig. 5a). Therefore the lattice constant of the *Pt–Al*$_{60}$ sample was calculated from the XRD pattern to $a = 3.9228(8)$ Å, using Werner's algorithm [25]. This is in agreement with the lattice constant of Pt ($a = 3.924$ Å) and thus matches the observed diffraction peaks clearly to platinum.

The fact that the presence of aluminum (as determined by EDX) cannot be detected by XRD suggests that aluminum does not form the genuine $Pt_{0.9}Al_{0.1}$ phase in the investigated samples, but is rather included statistically into the Pt-lattice. Since the inclusion of aluminum into a platinum lattice leads to a smaller lattice constant, this also explains the tailing of the observed diffraction peaks towards higher values of 2Θ (indicated by arrows A in Fig. 5a).

In terms of the electrode's biocompatibility the presence of approximately 10 at.% aluminum in the electrode renders the leaching of trace amounts particularly important. After operating the *Pt–Al*$_{60}$ cathode for 10 days in 100 ml of testing solution an aluminum concentration of (4 ± 1) μg L^{-1} was found. This is in the range of serum normal concentrations (0.5–35 μg L^{-1} [26,27]). Due to the small testing volume of 100 ml the employed experimental procedure results in an approximately 15-fold concentration of aluminum as compared to actual operation of the fuel cell in a body tissue environment (see Section 2.3). Considering this it can be expected that aluminum leaching upon operation will not significantly affect physiological normal levels.

3.2. Glucose tolerance and oxygen reduction performance

3.2.1. Influence of fabrication parameters on glucose tolerance

The results from the multi-step chronopotentiometry at 3.5% oxygen saturation, given as open circuit potential and area specific resistance with and without 3 mM glucose, are summarized in Table 1.

In the absence of glucose, the investigated samples show open circuit potentials between (332 ± 16) mV (*Pt–Al*$_{240}$), and (259 ± 13) mV (*Pt–Al*$_{120}$) vs. SCE, which indicates their general catalytic activity for oxygen reduction. Under load, *Pt–Al*$_{60}$ and *Pt–Al*$_{240}$ show similar area specific resistances of (19.0 ± 2.2) and (15.5 ± 1.2) kΩ cm^2, respectively. In contrast, at (39.7 ± 4.0) kΩ cm^2 *Pt–Al*$_{120}$ exhibits a more than two times larger value. Since XRD and EDX analyses revealed no significant difference between the investigated samples, we attribute this difference to the influence of annealing time on electrode morphology (see also Figs. 3 and 4).

Upon the addition of glucose to the testing solution the samples exhibit a decrease in open circuit potential between (32 ± 12) mV (*Pt–Al*$_{120}$) and (127 ± 11) mV (*Pt–Al*$_{240}$). This can be attributed to

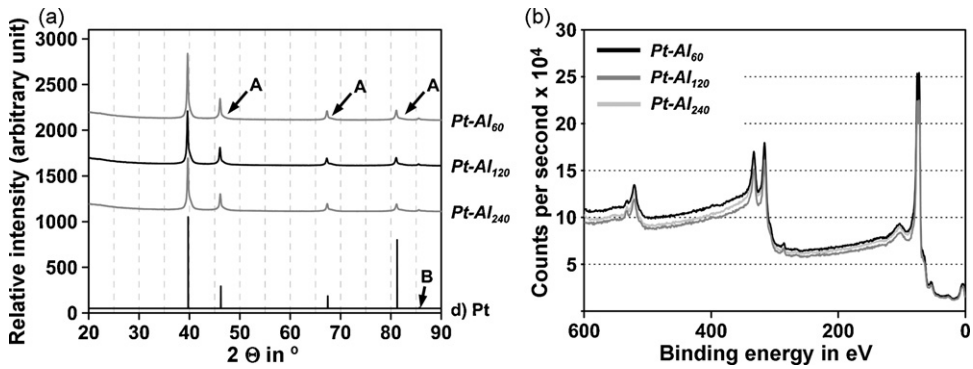

Fig. 5. (a) XRD patterns shown for *Pt–Al*$_{60}$, *Pt–Al*$_{120}$, and *Pt–Al*$_{240}$, as indicated in the figure. Reference data for Pt is taken from the ICSD [24]. Arrows A indicate peak tailing towards higher values of 2Θ, arrow B shows the position of the small platinum peak not visible at this scale. (b) XPS spectra of the samples recorded after 10 s of Ar-sputtering. The spectra do not significantly differ from spectra recorded after 5 s of Ar-sputtering (data not shown).

the catalytic activity of platinum towards glucose oxidation and the consequent formation of a mixed electrode potential between the redox potentials of oxygen reduction and glucose oxidation. The magnitude of glucose sensitivity also depends on annealing time. Here *Pt–Al*$_{240}$ exhibits the highest glucose sensitivity: its open circuit potential decreases by (127 ± 11) mV and the area specific resistance increases from (15.5 ± 1.2) to (50.6 ± 7.2) kΩ cm^2 once glucose is present in the solution. Although the open circuit potential of *Pt–Al*$_{120}$ shows the lowest sensitivity towards the presence of glucose (decrease of only (32 ± 12) mV), these samples exhibit a similarly high area specific resistance of (54.2 ± 8.8) kΩ cm^2. At (246 ± 3) mV *Pt–Al*$_{60}$ shows the highest open circuit potential in the presence of glucose. Compared to the previous cathodes based on activated carbon this value is approximately 86 mV more positive. Furthermore, under load the low glucose sensitivity of *Pt–Al*$_{60}$ is maintained, which at only (22.3 ± 3.0) kΩ cm^2 shows the lowest area specific resistance in the presence of glucose among the investigated samples. As shown in Section 3.1, *Pt–Al*$_{60}$ also exhibits the lowest trench density. Considering that both, EDX and XRD analysis revealed no significant difference between the catalytically active material resulting upon different annealing times, this suggests that glucose sensitivity is governed by mixed potential formation resulting from oxygen depletion within the trenches.

In summary, among the investigated samples *Pt–Al*$_{60}$ electrodes show the best performance under physiological concentrations of glucose (3 mM) and oxygen (7%), which renders them a promising candidate for application in abiotically catalyzed glucose fuel cells. Their more detailed characterization is presented in the following.

3.2.2. Influence of a protective Nafion coating

The electro-coated Nafion layer is intended to act as a diffusion barrier for glucose and other endogenous substances and thus diminish their interference on oxygen reduction at the cathode. In Fig. 6 the oxygen reduction performance of *Pt–Al*$_{60}$ with and without protective Nafion coating is compared in terms of current density–potential plots at 3.5% and 7.0% oxygen saturation. Compared to the results presented in the previous section, these plots were recorded by performing a multi-step chronoamperometry experiment with both, smaller load steps and longer hold time at a defined load current (see Section 2.5 for details). In general, the presence of a Nafion coating results in slightly more positive electrode potentials, under both open circuit and load conditions. This is attributed to the perm-selective characteristics of Nafion, hindering to some degree the access of glucose to the electrode and thus reducing the extent of mixed potential formation.

The magnitude of electrode potential increase due to the Nafion coating depends on both, the oxygen saturation in the testing solution and the applied load current. Regarding the situation at 7.0% oxygen saturation, the open circuit potential of Nafion-coated electrodes is by approximately 50 mV more positive. Under load this difference gradually decreases to approximately 44 mV at a current density of 4.4 μA cm^{-2}. Above 8.8 μA cm^{-2} both coated and non-coated electrodes show essentially the same performance. At 3.5% oxygen the difference in open circuit potential between coated and un-coated samples is noticeably reduced to approximately 23 mV, while at current densities above 8.8 μA cm^{-2} the curves coincide. The decreasing performance advantage of Nafion-coated electrodes at higher current densities and lower oxygen saturation can be attributed to the increasing dominance of oxygen mass transfer on the electrode reaction. This is corrugated by a comparison of electrode performance at the two different oxygen saturations: here an increase in oxygen partial pressure leads to reduced electrode polarization (Fig. 6).

For comparison, Fig. 6 shows also the polarization curves of state-of-the-art activated carbon cathodes [8], operated at the higher glucose concentration of 5.0 mM and without a diffusion barrier in front. Under load at 7.0% oxygen saturation the novel *Pt–Al*$_{60}$ cathodes show more positive potentials for current densities of up to 6.7 μA cm^{-2}, despite the additional diffusion barrier. This can be attributed to the higher catalytic activity of platinum as compared to activated carbon. Due to the increasing dominance of oxygen availability the catalytic advantage of platinum is less prominent at the lower oxygen concentration of 3.5%.

Table 1
Open circuit potentials and area specific resistances at 3.5% oxygen saturation of differently fabricated cathodes (triplicate experiments, mean value ± sample standard deviation).

Sample designation	Annealing parameters	Open circuit potential (mV) vs. SCE Glucose concentration		Area specific resistance (kΩ cm^2) Glucose concentration	
		0 mM	3.0 mM	0 mM	3.0 mM
Pt–Al$_{60}$	60 min at 300 °C	294 ± 6	246 ± 3	19.0 ± 2.2	23.3 ± 3.0
Pt–Al$_{120}$	120 min at 300 °C	259 ± 13	227 ± 2	39.7 ± 4.0	54.2 ± 8.8
Pt–Al$_{240}$	240 min at 300 °C	332 ± 16	205 ± 10	15.5 ± 1.2	50.6 ± 7.2

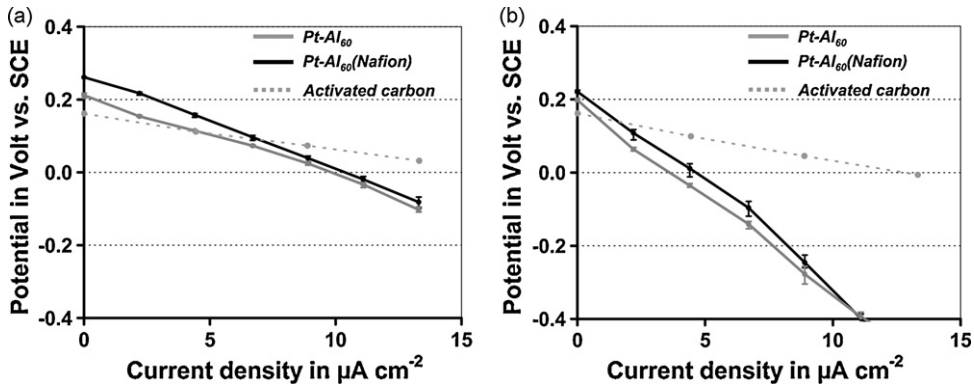

Fig. 6. Current density–potential curves of *Pt–Al*$_{60}$ cathodes in PBS with 3.0 mM glucose at (a) 7.0% and (b) 3.5% oxygen saturation (with and without perm-selective Nafion coating, as indicated). Given are the average values of triplicate experiments, bars represent maximum and minimum values. For comparison the polarization curve of an activated carbon cathode operated without a diffusion barrier is shown.

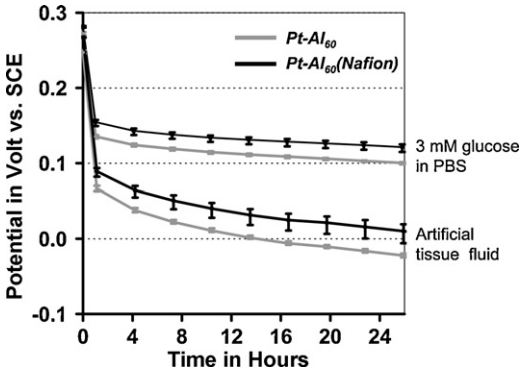

Fig. 7. Chronopotentiometry response of *Pt–Al*$_{60}$ cathodes with and without protective Nafion coating at a current density of 4.4 μA cm^{-2}. Curves recorded at 7.0% oxygen saturation either in PBS with 3.0 mM glucose or artificial tissue fluid (as indicated). Given are the average values of triplicate experiments, bars represent maximum and minimum values.

The results from chronopotentiometry experiments at a current density of 4.4 μA cm^{-2}, both in PBS with 3.0 mM glucose and artificial tissue fluid are shown in Fig. 7. Also under these conditions the protective characteristics of the Nafion coating are maintained. Upon exchange of the glucose solution against artificial tissue fluid, the Nafion-coated samples exhibit a potential decrease of (18 ± 1) mV, compared to (30 ± 1) mV with non-coated electrodes (values recorded 4 h after exchange of the solution, data not shown). After 26 h of continuous operation in artificial tissue fluid, the potential difference between coated and non-coated samples amounts to approximately 32 mV. Compared to operation in PBS containing 3 mM glucose, artificial tissue fluid leads to a potential decrease of approximately 120 mV for non-coated and 90 mV for the Nafion-protected cathodes. The coating in its present form can thus alleviate the potential loss in artificial tissue fluid by only approximately 25%.

Regarding the stability of electrode potential under constant load the average potential drift rates between 26 and 23 h of operation in PBS containing 3×10^{-3} mol L^{-1} glucose amount to −0.8 and −0.9 mV h^{-1} for cathodes with and without Nafion coating, respectively. This is in the range of the values encountered with hydrogel-bound activated carbon cathodes [8], and can be attributed to the slow load change behavior of the electrodes. In artificial tissue fluid the drift rates are higher, amounting to 1.9 and 1.8 mV h^{-1} for samples with and without Nafion coating, respectively. Considering that Raney-platinum film anodes operated in the same artificial tissue fluid show an approximately five times higher drift rate [2] this is nevertheless a promising result. Furthermore, it has to be considered that after 24 h of operation the artificial tissue fluid may already have started to undergo partial decomposition.

4. Conclusion

We demonstrated the fabrication and application of thin layer Raney-platinum films as glucose-tolerant cathodes for oxygen reduction in implantable glucose fuel cells. The main advantage of the novel cathodes over previous approaches is their excellent resistance against hydrolytic and oxidative attack (demonstrated by acid treatment as integral part of the fabrication process) and amenability to specific surface modification with protective polymers. Together with the Raney-platinum anodes presented in part 1 of this paper series [2], the present work is thus a fundamental step towards the realization of implantable glucose fuel cells that obviate the use of chemically instable hydrogel binders [28] in electrode fabrication.

With *Pt–Al*$_{60}$ annealed for 60 min at 300 °C a platinum-based electrode has been identified that shows sufficient glucose tolerance to be effectively used as cathode under physiological concentrations of glucose and oxygen, showing slightly more positive electrode potentials than hydrogel-bound activated carbon cathodes. Our initial hypothesis that the formation of a mixed potential between glucose and oxygen at platinum electrodes can be minimized by the construction of very thin electrodes has thus been verified. The results suggest that glucose sensitivity is governed by mixed potential formation resulting from oxygen depletion within the trenches, rather than material-intrinsic properties. However, further research will be required to fully clarify the phenomenon of glucose tolerance.

Under physiological conditions the presence of artificial tissue fluid results in a potential loss of approximately 120 mV under load as compared to operation in PBS. This loss can only to a limited extent (∼25%) be alleviated by the protective Nafion coating in its present form. We expect that a careful optimization of annealing parameters, alloying partners, and Nafion deposition will lead to further improvements. A promising strategy to improve poisoning resistance of the electrodes may also be catalyst refinement by surface modification or the formation of multi-component alloys (see, e.g. [29] and references therein).

Finally, our experiments indicate that aluminum release from the cathode will not significantly affect physiological normal levels. While this is a promising first result, dedicated cytotoxicity studies to evaluate the cathode's biocompatibility will be inevitable. The application of the here presented anodes in a complete fuel cell will be reported on in a subsequent publication [30].

Acknowledgements

We gratefully acknowledge financial support from the European Union (contract no. 001837 Healthy Aims), from the Deutsche Forschungsgemeinschaft (DFG) through the PhD program "Micro Energy Harvesting" (GRK 1322), and from the Ministry for Science, Research, and Arts of the Federal State Baden-Württemberg (co-operation Project "Biopower"). Also, we would like to thank Herbert Straatman (HSG-IMIT) for the preparation of cross-sections and electron microscope images, as well as Daniela Mössner (IMTEK – Laboratory for Chemistry and Physics of Interfaces) for recording the XPS spectra.

References

[1] S. Kerzenmacher, J. Ducrée, R. Zengerle, F. von Stetten, J. Power Sources 182 (2008) 1–17.
[2] S. Kerzenmacher, M. Schroeder, R. Brämer, R. Zengerle, F. von Stetten, J. Power Sources 195 (2010) 6516–6523.
[3] U. Gebhardt, J.R. Rao, G.J. Richter, J. Appl. Electrochem. 6 (1976) 127–134.
[4] A. Kozawa, V.E. Zilionis, R.J. Brodd, J. Electrochem. Soc. 117 (1970) 1474–1478.
[5] A. Kloke, B. Biller, U. Kräling, R. Zengerle, F. von, Stetten, Proceedings of the Eurosensors XXII Conference 2008, Dresden, Germany, 2008, pp. 1416–1419.
[6] P. Malachesky, G. Holleck, F. McGovern, R. Devarakonda, Proceedings of the 7th Intersociety Energy Conversion Engineering Conference, 1972, pp. 727–732.
[7] S.K. Wolfson, S.L. Gofberg, P. Prusiner, L. Nanis, Trans. Am. Soc. Artif. Int. Organs 14 (1968) 198–203.
[8] S. Kerzenmacher, J. Ducrée, R. Zengerle, F. von Stetten, J. Power Sources 182 (2008) 66–75.
[9] J.R. Rao, G. Richter, F. von Sturm, E. Weidlich, Ber. Bunsen-Ges.—Phys. Chem. Chem. Phys. 77 (1973) 787–790.
[10] J.R. Rao, G. Richter, F. von Sturm, E. Weidlich, M. Wenzel, Biomed. Eng. 9 (1974) 98–103.
[11] R.F. Drake, B.K. Kusserow, S. Messinger, S. Matsuda, Trans. Am. Soc. Artif. Int. Organs 16 (1970) 199–205.
[12] E. Aschasuer, R. Fasching, M. Varahram, G. Jobst, G. Urban, G. Nicolussi, W. Husinsky, G. Friedbacher, M. Grasserbauer, J. Electroanal. Chem. 426 (1997) 157–165.
[13] E. Aschauer, R. Fasching, G. Urban, G. Nicolussi, W. Husinsky, J. Electroanal. Chem. 381 (1995) 143–150.
[14] P.D. van der Wal, M. Dadras, M. Koudelka-Hep, N.F. de, Rooij, ECS Meeting Abstracts, Honolulu, Hawaii, 2004, p. 495.
[15] S.P. Murarka, I.A. Blech, H.J. Levinstein, J. Appl. Phys. 47 (1976) 5175–5181.
[16] D. Moattisirat, V. Poitout, V. Thome, M.N. Gangnerau, Y. Zhang, Y. Hu, G.S. Wilson, F. Lemonnier, J.C. Klein, G. Reach, Diabetologia 37 (1994) 610–616.
[17] M.P. Brazell, R.J. Kasser, K.J. Renner, J. Feng, B. Moghaddam, R.N. Adams, J. Neurosci. Methods 22 (1987) 167–172.
[18] Y.J. Lee, D.J. Park, J.Y. Park, IEEE Sens. J. 8 (2008) 1922–1927.
[19] A.A. Sharkawy, B. Klitzman, G.A. Truskey, W.M. Reichert, J. Biomed. Mater. Res. 37 (1997) 401–412.
[20] E.L. Cussler, in: E.L. Cussler (Ed.), Diffusion, Mass Transfer in Fluid Systems, Cambridge University Press, Cambridge, UK, 2009, pp. 13–47.
[21] W.W. Webster, S.F. Stinson, W.H. Wong, Clin. Chem. 17 (1971) 1050–1054.
[22] S. Kerzenmacher, K. Mutschler, U. Kräling, H. Baumer, J. Ducrée, R. Zengerle, F. von, Stetten, J. Appl. Electrochem. 39 (2009) 1477–1485.
[23] Y. Oya, Y. Mishima, T. Suzuki, Z. Metallkd. 78 (1987) 485–490.
[24] A. Belsky, M. Hellenbrandt, V.L. Karen, P. Luksch, Acta Crystallogr. B—Struct. Sci. 58 (2002) 364–369.
[25] P.E. Werner, L. Eriksson, M. Westdahl, J. Appl. Crystallogr. 18 (1985) 367–370.
[26] H. Valentin, P. Preusser, K.H. Schaller, Int. Arch. Occup. Environ. Health 38 (1976) 1–17.
[27] S. Caroli, A. Alimonti, E. Coni, F. Petrucci, O. Senofonte, N. Violante, Crit. Rev. Anal. Chem. 24 (1994) 363–398.
[28] J.R. Rao, G.J. Richter, F. von Sturm, E. Weidlich, Bioelectrochem. Bioenerg. 3 (1976) 139–150.
[29] J. Shim, D.Y. Yoo, J.S. Lee, Electrochim. Acta 45 (2000) 1943–1951.
[30] S. Kerzenmacher, U. Kräling, T. Metz, R. Zengerle, F. von Stetten, J. Power Sources, submitted for publication.